

Numerical study of wake and aerodynamic forces on a twin-box bridge deck with different gap ratios

Jingmiao Shang^{1a}, Qiang Zhou^{*1}, Haili Liao^{1b}, Allan Larsen^{2c}, Jin Wang^{1d} and Mingshui Li^{1e}

¹Research Center for Wind Engineering, Southwest Jiaotong University, China

²COWI Consulting Engineers and Planners A/S, Denmark

(Received February 28, 2019, Revised November 15, 2019, Accepted December 4, 2019)

Abstract. Two-dimensional Delayed Detached Eddy Simulation (DDES) was carried out to investigate the uniform flow over a twin-box bridge deck (TBBD) with various gap ratios of $L/C=5.1\%$, 12.8% , 25.6% , 38.5% , 73.3% and 108.2% (L : the gap-width between two girders, C : the chord length of a single girder) at Reynolds number, $Re=4\times 10^4$. The aerodynamic coefficients of the prototype deck with gap ratio of 73.3% obtained from the present simulation were compared with the previous experimental and numerical data for different attack angles to validate the present numerical method. Particular attention is devoted to the fluctuating pressure distribution and forces, shear layer reattachment position, wake velocity and flow pattern in order to understand the effects of gap ratio on dynamic flow interaction with the twin-box bridge deck. The flow structure is sensitive to the gap, thus a change in L/C thus leads to single-side shedding regime at $L/C\leq 25.6\%$, and co-shedding regime at $L/C\geq 35.8\%$ distinguished by drastic changes in flow structure and vortex shedding. The gap-ratio-dependent Strouhal number gradually increases from 0.12 to 0.27, though the domain frequencies of vortices shedding from two girders are identical. The mean and fluctuating pressure distributions is significantly influenced by the flow pattern, and thus the fluctuating lift force on two girders increases or decreases with increasing of L/C in the single-side shedding and co-shedding regime, respectively. In addition, the flow mechanisms for the variation in aerodynamic performance with respect to gap ratios are discussed in detail.

Keywords: twin-box bridge deck; Delayed Detached Eddy Simulation; vortex shedding; aerodynamic forces; gap ratios

1. Introduction

In order to improve the aerodynamic stability of long-span bridge, a kind of twin-box girder bridge deck section has been attracted in recent years (Larsen 1993, Diana *et al.* 2004, Ge and Xiang 2008, Fumoto and Watanabe 2015) and applied in engineering, such as the Xihoumen suspension bridge (main span: 1650 m, China), the Stonecutters cable-stayed bridge (main span: 1018 m, Hong Kong), the Gwangyang suspension bridge (main span: 1545 m, Korea), as well as the longest span bridge under construction - the 1915 Canakkale Bridge (main span: 2023 m, Turkey).

The twin box deck and a single box deck have different aerodynamic characteristics and the gap ratio of a twin box

deck has significant effects on its aerodynamic behaviour, which has been proved by previous theoretical and experimental studies (Ogawa *et al.* 2002, Qin *et al.* 2007, Liu *et al.* 2009, Zhu and Xu 2014). As for the flutter stability, dividing the deck into two parts by the central gap has a positive effect due to a higher critical flutter wind speed. However, there has been some disagreement on the results of the most effective gap ratio. Larsen (1993) found that the critical flutter wind speed increased with the gap width in the Gibraltar Bridge. Similarly, Sato *et al.* (2000) studied the effect of gap width on flutter performance by section model wind tunnel tests and found that the flutter onset wind speed was increased with the gap width. Yang and Ge (2009) indicated that there is a maximum flutter critical wind speed at critical gap width, and then it decreases with increasing of the gap width in their case study of the twin-box deck of Xihoumen suspension Bridge. This disagreement may be due to the unclear understanding of the flow interaction and mechanism of the gap ratio. In addition, the vortex-induced vibration (VIV) tends to arise for twin box girders due to the complicated flow around the box and gap as well as the interference between the two girders (Li *et al.* 2011, Chen *et al.* 2013, Yang *et al.* 2016). Larsen *et al.* (2008) observed the obvious VIV of the Stonecutters Bridge, which has a twin box girder section, and experimentally investigated the suppression effect of guide vanes. Li *et al.* (2011) investigated the VIV of a twin steel box girder of Xihoumen Bridge based on field measurements, and indicated that the VIV more likely

*Corresponding author, Ph. D
E-mail: milan1023@gmail.com

^aPh.D. Student
E-mail: mervin@my.swjtu.edu.cn

^bProfessor
E-mail: hlliao@swjtu.edu.cn

^cProfessor
E-mail: aln@cowi.dk

^dPh. D
E-mail: wangjin198927@outlook.com

^eProfessor
E-mail: lms_rcwe@126.com

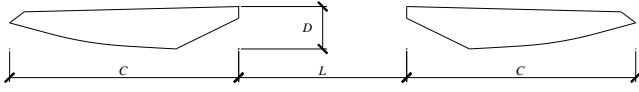


Fig. 1 Geometric information of the TBBD with various gap ratios

occurs in a low wind speed range of 6 ~ 10 m/s. Chen *et al.* (2014) studied the wind-induced vortex shedding of two parallel box-girder bridges using wind tunnel tests.

As mentioned above, the gap ratio has significant effects on the aerodynamics and aeroelastics of twin-box girders. However, the flow mechanism of gap ratio is still unclear. Thus Kwok *et al.* (2012) studied the effects of gap ratio on aerodynamic characteristics of twin-box girders of Stonecutters bridge by wind tunnel tests. Laima and Li (2015) investigated experimentally the vortex shedding and the time-averaged pressure/forces of Xihoumen bridge deck. However, less attention is devoted to the fluctuating pressure/forces, flow pattern, as well as their relationship.

On the other hand, more and more researchers have been investigating the aerodynamic behaviour of a twin-box deck using computational fluid dynamic (CFD) methods. Zhang *et al.* (2017) investigate the nonlinear aerodynamic of twin-box girder bridge deck sections from the viewpoint of energy by a two-dimensional (2D) numerical study. Nieto *et al.* (2010) performed a URANS study to investigate the vortex-shedding response of a twin box deck. Li *et al.* (2018) performed 2D delayed detached eddy simulation (DDES), which is the hybrid approach combining LES and RANS, to investigate the aerodynamic mechanism behind the suppression of vortex-induced vibrations (VIVs) of twin box girders by central grids.

The aforementioned investigations on the flow around twin box girders shown that the numerical approach has become more popular and can be successful, even though most of these numerical studies were only 2D. However, how the fluctuating pressure distribution, fluctuating forces, wake structure and flow pattern, as well as their relationship, have been paid little attention. Thus a static twin-box bridge deck with different gap ratios, which are same to those in the previous experiment of Kwok *et al.* (2012), was chosen as the objective deck, and 2D DDES simulations were performed to investigate the wake and aerodynamic forces at Reynolds number $Re=UD/v=4 \times 10^4$, where U is the free stream velocity, D is the height of the bridge deck, and v is the kinematic viscosity. The prototype we focused is a twin-box cable-stayed bridge with a main span of 1018 m. As shown in Figure 1, the chord length (C) of a single girder and height of the bridge deck at the mid-span location are 19.5 m and 3.5 m, respectively. Six simulation configurations were investigated, with the gap-width (L) between two girders to the chord length of a single girder ratios of $L/C=5.1\%$, 12.8% , 25.6% , 38.5% , 73.3% and 108.2% , corresponding to prototype scale gap-widths of 1 m, 2.5 m, 5 m, 7.5 m, 14.3 m and 21.1 m. The numerical method and numerical details applied in this study are validated by comparing with the aerodynamics of a wind tunnel test at the same Reynolds number. Then, the Strouhal number, time-averaged and instantaneous flow

structures, pressure distributions and forces on the twin-box bridge deck, as well as their relationship, are investigated in detail in order to understand the interaction and underlying mechanism of the flow around twin-box bridge deck with different gap ratios.

2. Numerical setup

2.1 Governing equations

Detached Eddy Simulation (DES) is a hybrid approach combining LES and RANS proposed by Spalart and Allmaras (1992) and Spalart *et al.* (1997). It means that the regions near solid boundaries and where the turbulent length scale is less than the maximum grid dimension, the RANS mode of solution is applied. The free flow regions are solved using the LES mode as the turbulent length scale exceeds the grid dimension. The method is expected to accurately simulate the wall-bounded turbulent flows at high Reynolds numbers. To improve the performance of model on the flows with strong adverse pressure gradient and large regions of separation, Menter (1994) further developed a one-equation DES model based on the standard $k-\omega$ SST model. The standard $k-\omega$ SST model can be written as

$$\frac{\partial(\rho k)}{\partial t} + \frac{\partial(\rho u_j k)}{\partial x_j} = P - \beta^* \rho \omega k + \frac{\partial}{\partial x_j} [(\mu + \sigma_k \mu_t) \frac{\partial k}{\partial x_j}] \quad (1)$$

$$\frac{\partial(\rho \omega)}{\partial t} + \frac{\partial(\rho u_j \omega)}{\partial x_j} = \frac{\gamma}{v_t} P - \beta \rho \omega^2 + \frac{\partial}{\partial x_j} [(\mu + \sigma_\omega \mu_t) \frac{\partial \omega}{\partial x_j}] + 2(1 - F_1) \frac{\rho \sigma_{\omega 2}}{\omega} \frac{\partial k}{\partial x_j} \frac{\partial \omega}{\partial x_j} \quad (2)$$

$$F_1 = \tanh(\arg_1^4), \arg_1 = \min \left[\max \left(\frac{\sqrt{k}}{\beta^* \omega d}, \frac{500v}{d^2 \omega} \right), \frac{4\rho \sigma_{\omega 2} k}{CD_{k\omega} d^2} \right] \quad (3)$$

$$\mu_t = \frac{\rho a_1 k}{\max(a_1 \omega, \Omega F_2)} \quad (4)$$

$$F_2 = \tanh(\arg_2^2), \arg_2 = \max \left(2 \frac{\sqrt{k}}{\beta^* \omega d}, \frac{500v}{d^2 \omega} \right) \quad (5)$$

where d is the distance to the nearest wall and ω is the vorticity, SST closure constants $\beta^*=0.09$, $a_1=0.31$.

The DES modification presented by Menter is meant to switch the turbulent length scale from a RANS length scale to a LES length scale when the grid is sufficiently fine. The turbulent length scale L_t is given by

$$L_t = \frac{k^{3/2}}{\varepsilon} = \frac{\sqrt{k}}{\beta^* \omega} \quad (6)$$

As the grid is refined below the limit $\Delta_{max} < L_t$, the DES-limiter is activated and switches the model from RANS to LES mode. Δ_{max} is the maximum local grid spacing. The intention of the model is to run in RANS mode for attached flow regions, and to switch to LES mode in detached regions away from walls.

The DES limiter is activated by grid refinement inside

the attached boundary layers, while it may affect the RANS model by reducing the computed eddy viscosity which can lead to grid-induced separation, as discussed by Menter *et al.* (2003), where the boundary layers separates at arbitrary locations based on the grid spacing. In order to avoid this, the DES concept has been extended to Delayed-DES (DDES), following the proposal of Menter *et al.* to 'shield' the boundary layer from the DES limiter Shur *et al.* (2008). The dissipation term in the k -equation is then re-formulated as follows

$$E_{DES} = \rho \frac{k^{3/2}}{\min(L_t, C_{DES}\Delta_{max})} = \quad (7)$$

$$\rho \frac{k^{3/2}}{L_t} \max\left(\frac{L_t}{C_{DES}\Delta_{max}}, 1\right) = \rho \frac{k^{3/2}}{L_t} F_{DES}$$

$$F_{DES} = \max\left[\frac{L_t}{C_{DES}\Delta_{max}} \cdot (1 - F_{DDES}), 1\right] \quad (8)$$

The F_{DDES} blending function is given by

$$F_{DDES} = \tanh[(C_{d1}r_d)^{C_{d2}}] \quad (9)$$

where $C_{d1} = 20$, $C_{d2} = 3$, and

$$r_d = \frac{v_t + \nu}{\kappa^2 y^2 \sqrt{0.5 \cdot (S^2 + \Omega^2)}} \quad (10)$$

where S is the magnitude of the strain rate tensor, Ω is the magnitude of vorticity tensor, y is the wall distance, and $\kappa = 0.41$.

DDES detects boundary layers and prolongs the full RANS model, even if the wall-parallel grid spacing would normally activate the DES limiter. DDES model is less sensitive to the near-wall grid arrangement.

2.2 Numerical discretization and algorithm

In the simulation, the velocity and pressure are defined at the center of a control volume, while the volume fluxes are defined at the midpoint of their corresponding cell surfaces. The momentum interpolation method is used to avoid oscillating problems by eliminating the checkerboard pressure and subsequent refinements with a non-staggered mesh. The fractional step method (FSM) algorithm proposed by Armfield and Street (1999) is utilized. With the Non-Iterative Time Advancement Solution Method (NITA) scheme, the FSM is slightly less computationally expensive compared to the PISO algorithm. The FSM achieves the same order of accuracy as the iterative method with a considerable increase in efficiency. By making the factorization error commensurate with the leading truncation error arising from the second-order temporal discretization, the FSM preserves a second-order temporal accuracy without costly global iterations per each time-step Kim and Makarov (2005). That is why we select this algorithm for the present work. In addition, the residual tolerance of the non-iterative solver controls of pressure and momentum are set to 1×10^{-9} and 1×10^{-8} , respectively.

To avoid the instability caused by central-differencing schemes and non-physical wiggles, the bounded central

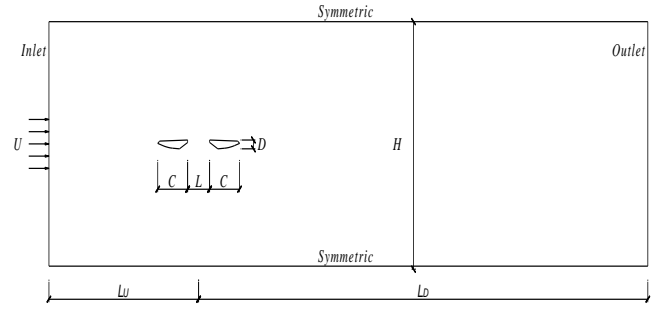


Fig. 2 Computational domain and boundary conditions

differencing scheme is applied to the spatial differencing of the convection term, which is a composite normalized variable diagram scheme Leonard (1991). Moreover, a fully implicit second-order time-advancement scheme is chosen for temporal discretization to obtain a stable and accurate simulation.

2.3 Computational domain and boundary conditions

The physical domain is shown in Fig. 2, where $LU=5C$, $LD=5C$ and $H=28.5D$ represent the distances from the inlet and outlet to the center of the gap, and the height, respectively. The blockage ratio is 3.5 %, which is smaller than the suggestion (6.4%) of Sohankar (2008).

Fig. 3 presents the grid system, where the structured O-type grid systems with the depth of the first grid near the body surface with empirical value of 0.0025 are applied to adequately resolve the flow. This maintains the maximum y^+ less than 1. For more efficient simulations, the computational domain is spatially resolved such that a dense clustering of grid points is applied near the wall, especially in the wake side, whereas a coarser grid is used away from the wall. Table 1 summarizes the cell numbers of all the cases. For the temporal discretization, the non-dimensional time-step $\Delta t^* = \Delta t U/D$ (Δt : time-step for calculation) is 1×10^{-4} , which maintains the Courant number less than 1.

The boundary conditions for simulation, illustrated in Fig. 2, are as follows:

- Inlet boundary: The uniform velocity condition without turbulence, $U=10$ m/s and $V=0$ is imposed, where U and V mean the streamwise velocity and vertical velocity at the inlet, respectively.
- Girders surface boundaries: A no-slip condition is imposed.
- Upper and lower boundaries: A symmetric condition (zero normal velocity and zero normal gradients of all variables) is applied.

Outlet boundary: A pressure outlet condition with zero static gauge pressure is imposed.

Table 1 Gap ratios and cell number

Item	Case 1	Case 2	Case 3	Case 4	Case 5	Case 6
L/C	5.1%	12.8%	25.6%	38.5%	73.3%	108.2%
Cell number	242775	253125	256575	258300	261750	265200

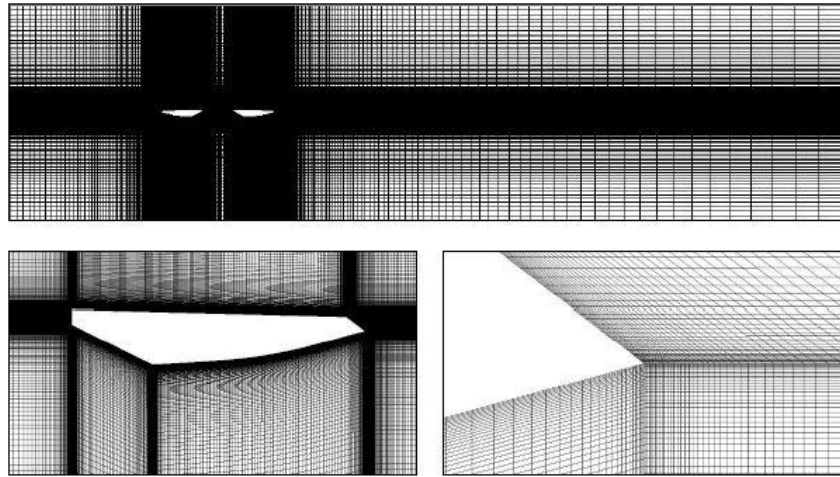


Fig. 3 Close-up view of grid system

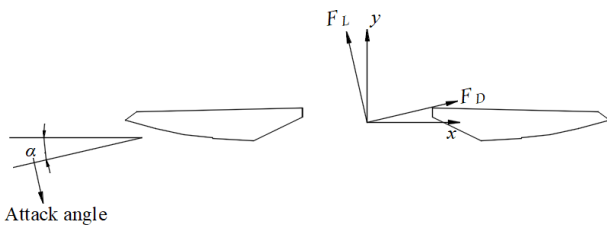


Fig. 4 Local coordinate system for the twin-box bridge deck

2.4 Numerical validation

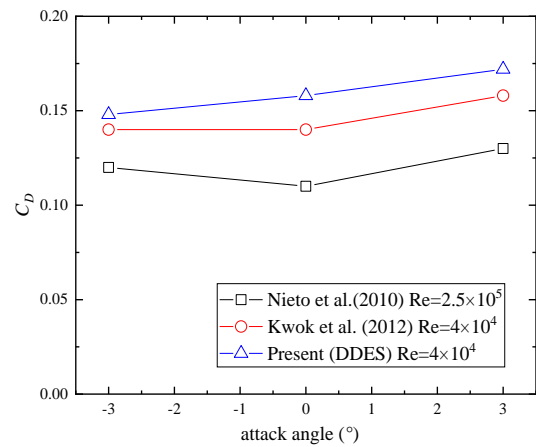
To validate the present simulation, basic aerodynamic parameters of the prototype of twin-box deck ($L/C=73.3\%$) with wind attack angles of -3° , 0° and $+3^\circ$ obtained by present numerical simulation are compared with those of previous numerical and experimental studies, where the aerodynamic coefficients are defined as in Eqs. (11) and (12) and they are consistently normalized by both the chord length C .

$$C_D = \frac{F_D}{0.5\rho U^2 C} \tag{11}$$

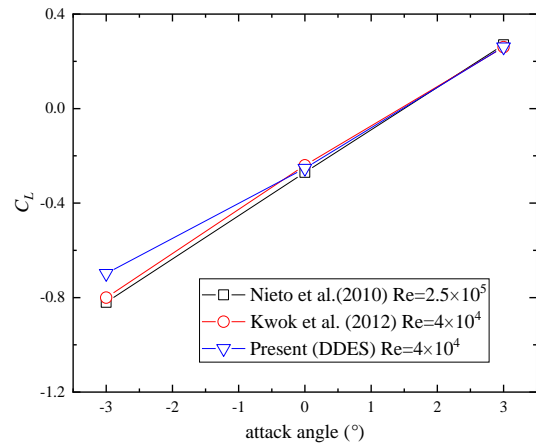
$$C_L = \frac{F_L}{0.5\rho U^2 C} \tag{12}$$

where C_D and C_L are the mean drag and lift coefficients, respectively. F_D and F_L are the drag and lift force on the per unit length of the bridge deck respectively. ρ is the flow density and U is the oncoming flow speed. The definition of coordinate system is depicted in Fig. 4.

As shown in Fig. 5, both the present numerical results and experimental results have similar variation with the attack angle. In addition, the mean drag coefficients obtained by the present simulation exhibits better agreement with the experimental results of Kwok *et al.* (2012) than Nieto *et al.* (2010), as shown in Fig. 5(a), with the average difference less than 6%. Fig. 5(b) shows that the mean lift coefficients with different angles of wind attack have reasonable agreement with each other, although there is



(a) Mean drag coefficient



(b) Mean lift coefficient

Fig. 5 Comparison of aerodynamic coefficients with various wind attack angles

little disparity for the results of wind attack angle of -3° .

In short, the numerical method and the grid system utilized in the present simulation provides reasonably good simulation results. Hence, the same numerical method and grid system is applied to the simulation of flow over the twin-box girders with different L/C .

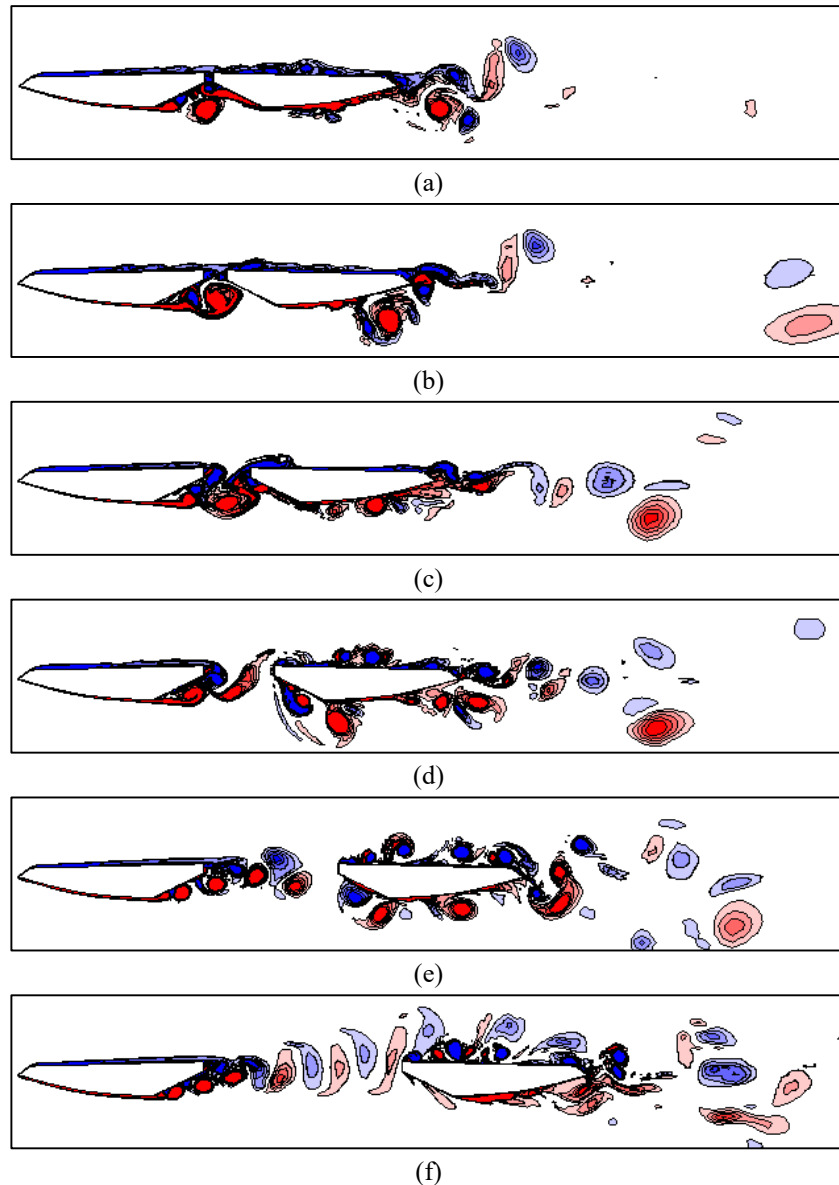


Fig. 6 Instantaneous streamwise vorticity contours in the case of $L/C =$ (a) 5.1%, (b) 12.8%, (c) 25.6%, (d) 38.5%, (e) 73.3%, and (f) 102.8%

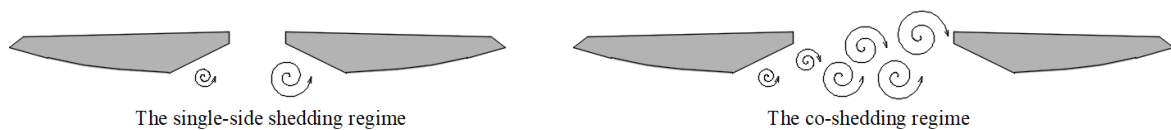


Fig. 7 Schematic of two different regimes

3. Results and discussion

3.1 Flow structures

Fig. 6 present the behaviour of the flow structures around twin-box girders with different gap ratios of 5.1%, 12.8%, 25.6%, 38.5%, 73.3% and 108.2% by illustrating the instantaneous streamwise vorticities ($\omega_z = -10 \sim 10$ with step of 2). The blue and red colours represent the clockwise and counter-clockwise vortices, respectively. All figures correspond to the moment where the lift coefficient is

maximum. The flow pattern around the twin-box girders with different gap ratios can be divided into two major regimes. As shown in Figs. 6(a) - 6(c), the shear layer from the lower surface of upstream girder rolls up, and the vortices mainly shed from this side. It indicates that no Karman vortex street appears in the gap as $L/C \leq 25.6\%$. Here this flow pattern is denoted as the single-side shedding regime. Laima and Li (2015) also found a similar phenomenon in their experimental study of another twin-box bridge deck, though they didn't discuss in detail. As the L/C increases to 38.5% in Fig. 6(d), the downstream girder

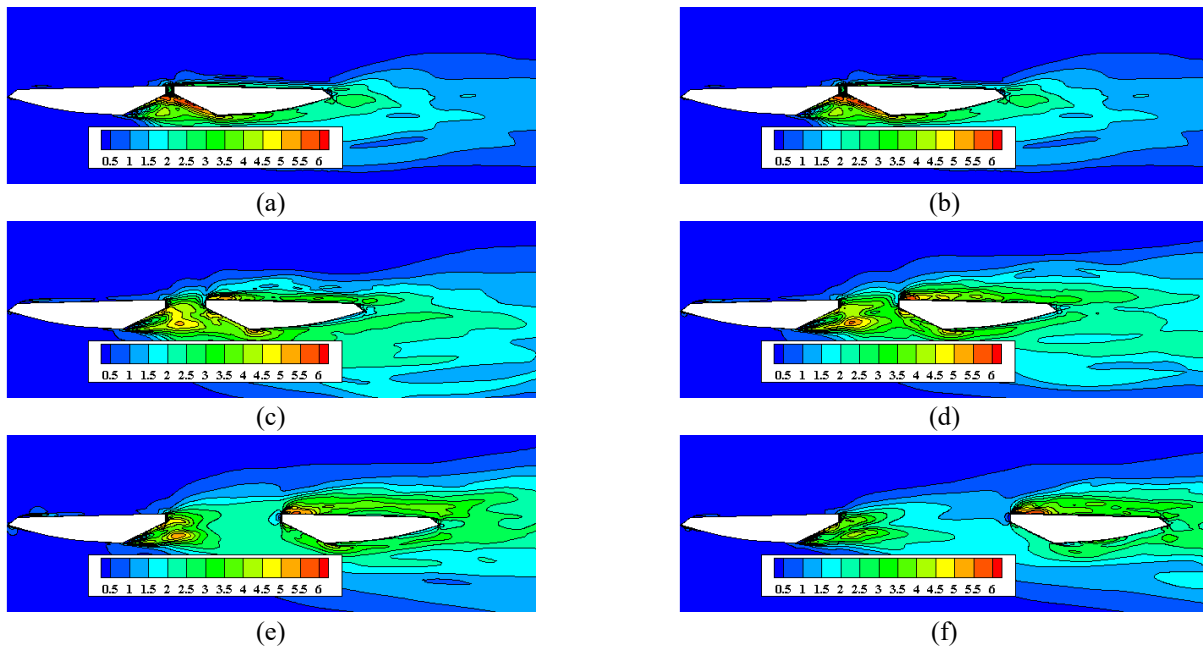


Fig. 8 RMS streamwise velocity contours in the case of $L/C =$ (a) 5.1%, (b) 12.8%, (c) 25.6%, (d) 38.5%, (e) 73.3% and (f) 102.8%

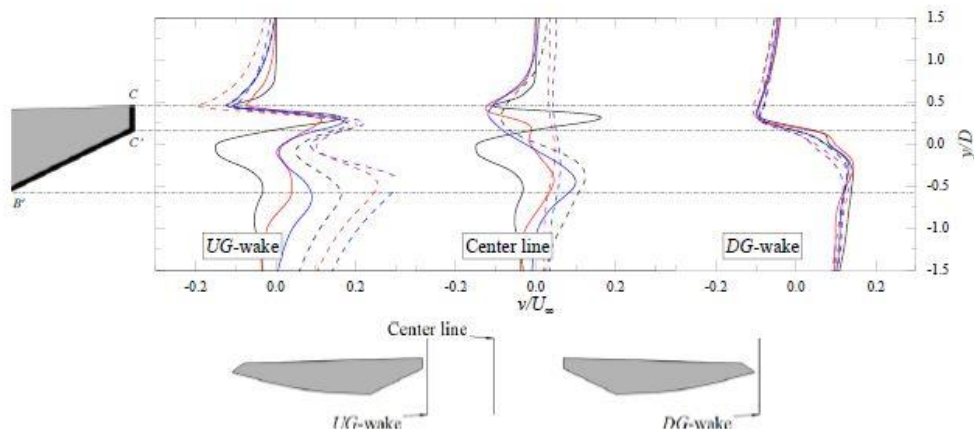


Fig. 9 Mean vertical velocity at three locations

Note: UG-wake means the location of 0.5 m from the rear corner of upstream girder, Center line means the center of the gap between two girders and DG-wake means the location of 0.5 m from the rear corner of upstream girder

is sufficiently far away to enable the shear layers from the both sides of the upstream girder roll up in the gap, where the alternate vortex shedding occurs. Thus it means that the binary vortex streets appear in the wakes of both girders. As these flow phenomena are similar to those of the co-shedding regime of two tandem circular cylinders (Zdravkovich 1986, Zhou and Yiu 2006, Zhou and Mahbub Alam 2016) and square cylinders (Sohankar 2012), this kind flow pattern in Figs. 6(d) - 6(f) is denoted the co-shedding regime in the present study. The vortex street in the wake of downstream girder is triggered by vortices in the gap and becomes apparently wider as in the co-shedding regimes, which is similar to those in the flow over two tandem circular cylinders (Sumner 2010). This change of flow pattern would have a significant influence on the wake structures and aerodynamic forces on both the upstream and

downstream girders as discussing later.

Fig. 8 shows the contours of fluctuating (RMS) streamwise velocity for different gap ratios. When $L/C \geq 38.5\%$, two distinct peaks can be observed as shown in Figs. 8(d) - 8(f), which illustrates a binary alternate vortex shedding occurring in the gap. Thus, it also means that the flow pattern changes to the co-shedding regime as L/C increases to 38.5%. Another significant phenomenon is the increased flow separation of the downstream girder due to the flow pattern changes. As shown in Figs. 8(a) - 8(c), the flow over the upstream girder close to the upper surface of the downstream one.

The profiles of mean vertical velocity at three locations with different L/C are shown in Fig. 9. For the UG-wake profile, the magnitude of the mean vertical velocity at the corner C and B' increases with increasing L/C which means

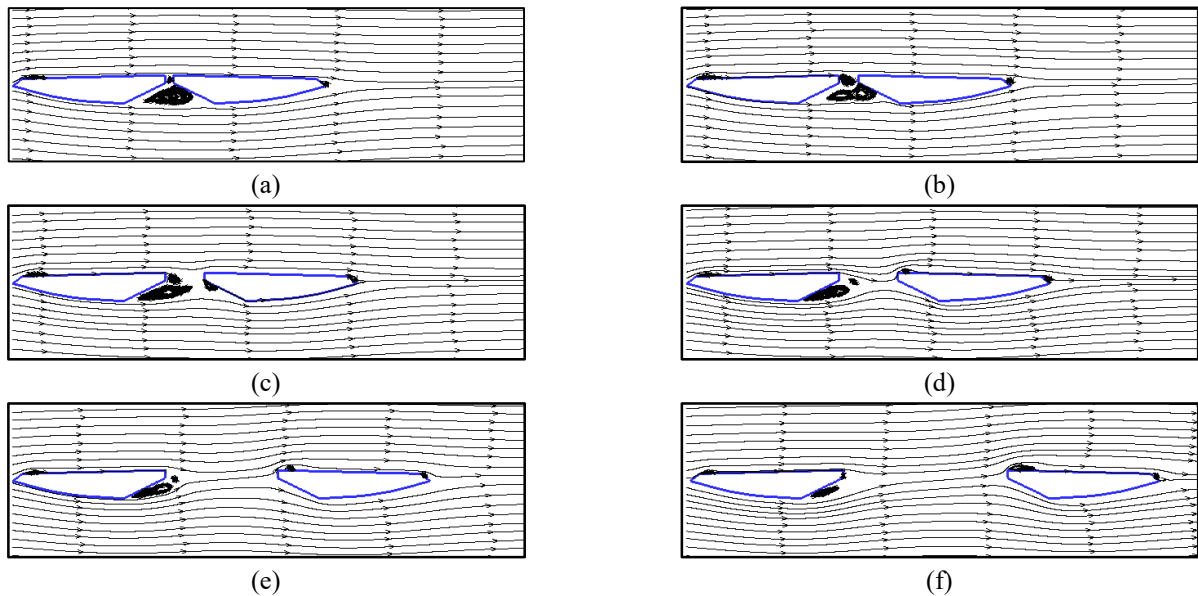
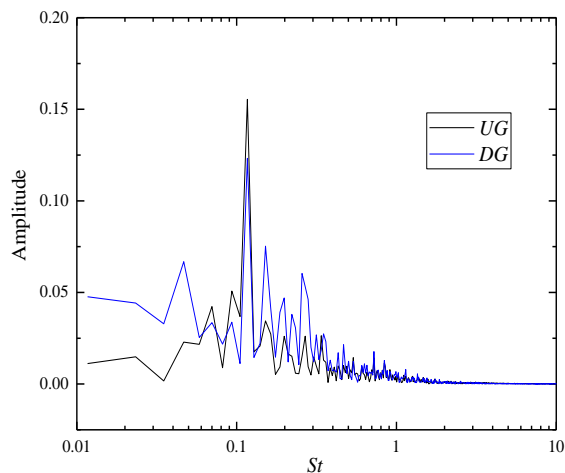
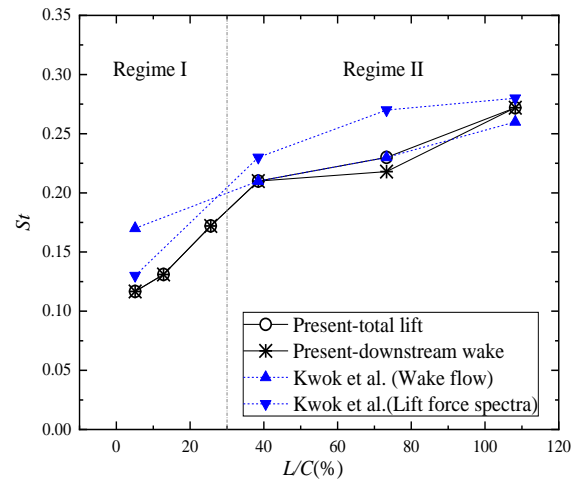


Fig. 10 Time-averaged streamlines in the case of L/C = (a) 5.1%, (b) 12.8%, (c) 25.6%, (d) 38.5%, (e) 73.3% and (f) 102.8%



(a) spectrum of lifts at $L/C=5.1\%$



(b) Strouhal number

Fig.11 Strouhal numbers for different gap ratios of L/C

the vortices shed from Side $B'-C'$ develop gradually. It can be found that the mean vertical velocities are positive for the L/C of 73.3% and 108.2% at the Center line, indicating that upward vertical velocity occurs, and the vortices shed from the upstream girder moves toward the upper surface of downstream girder. Moreover, it can be seen from the profile of DG -wake that the L/C has little or no effect on the mean vertical velocity of the downstream girder.

Fig. 10 shows the time-averaged streamline around the twin-box decks with various gap ratios. In the single-side shedding regime, there is a main eddy formed in the lower middle of the center gap, formed by the vortex shedding occurring in this area. As the flow pattern transforms into the co-shedding regime, two eddies with different sizes co-exists near to the leeward side of the upstream girder, which shows the appearance of vortices that are shed alternatively. With increasing L/C , the eddy gradually decreases and moves upward to the web of upstream girder,

which in turn affects the mean surface pressure distribution as discussed in the following section. In addition, when L/C increases to 38.5%, the eddy formed on the leading edge of upper surface of downstream girder appears more obvious and the separation bubble on the downstream windward side disappears, which may be due to the upward vertical velocity occurring in the gap as shown in Fig. 8. All the variations of streamlines with gap ratios would have significant influence on the characteristics of aerodynamic forces.

The Strouhal number (St) is defined as $St=f D/U$, where f has three definitions that are the dominant frequency of the total lift force and the dominant frequency of vortices shedding in the wakes of downstream girder, respectively. Fig. 11 shows the variation of St with L/C and it is compared with those of experimental study by Kwok *et al.* (2012) at the same Reynolds number.

The St gradually increases from 0.12 to 0.27 with L/C ,

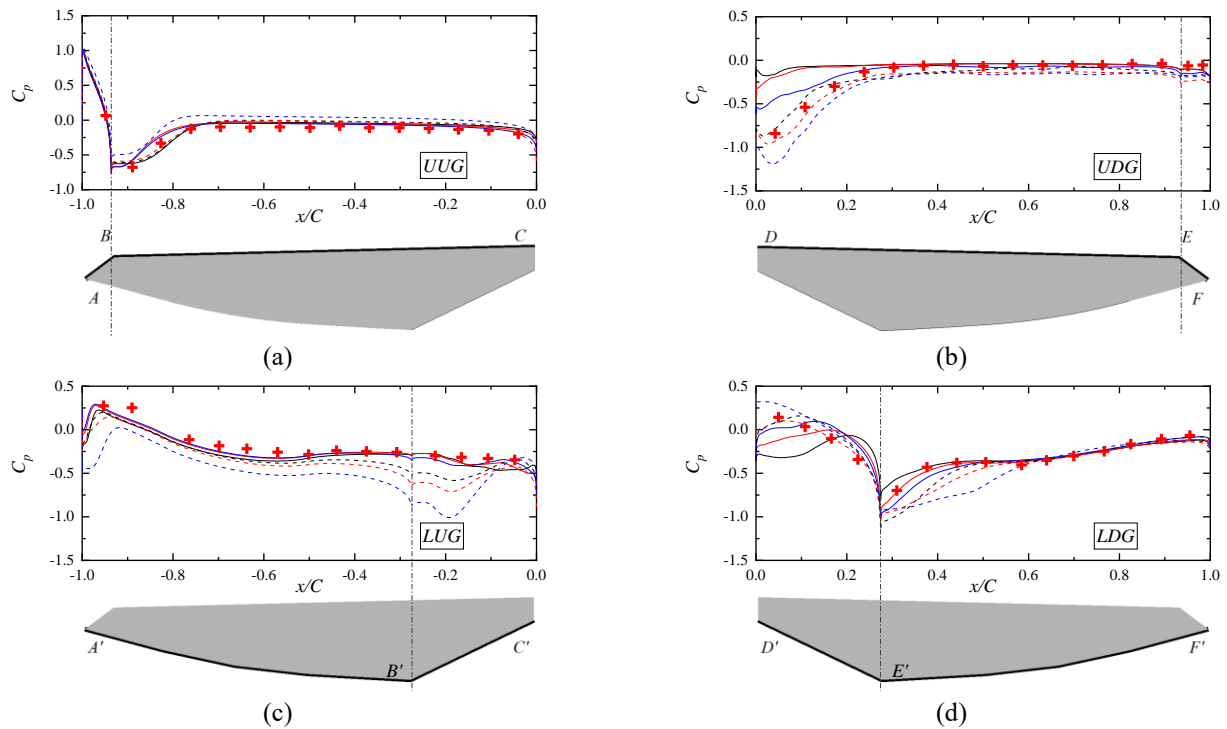


Fig.12 Mean pressure distributions along: (a) UUG, (b) UDG, (c) LUG and (d) LDG

*—: $L/C = 5.1\%$; —: $L/C = 12.8\%$; —: $L/C = 25.6\%$; ----: $L/C = 38.5\%$; -.-.: $L/C = 73.3\%$; -.-.-: $L/C = 108.2\%$; +: $L/C = 73.3\%$, Kwok *et al.* (2012).

Note: UUG means the upper surface of upstream girder; UDG means the upper surface of downstream girder; LUG means the lower surface of upstream girder and LDG means the lower surface of downstream girder.

which agrees well with the results of Kwok *et al.* (2012). The downstream girder, which is immersed in the wake of the upstream girder, is subjected to turbulence buffeting induced by the vortices shed from the upstream girder, and the downstream girder may affect the wake excitation of the upstream girder. Both the wake excitation and the turbulent buffeting are influenced by the L/C . For small gap ratios, the wake vortex shedding is not well developed because of the obstruction by downstream girder. As the L/C increases to 38.5%, the flow pattern changes from the single-side shedding regime to the co-shedding regime with the significant change, where the St changes suddenly in the curves with a hollow circle symbol in Fig. 9. When the two girders are separated sufficiently far apart, the vortex shedding mechanism is dominated by the two girders individually. In addition, the dominating frequencies of vortices shedding in the wakes of upstream and downstream girders are almost the same but the main vortex shedding of the twin girders are independent.

3.2 Aerodynamic forces

3.2.1 Surface pressure distribution

In order to understand the flow interaction and excitation mechanism of twin box girders, the pressure distribution around the bridge deck was investigated in detail. This method has been widely employed in previous studies of bluff body aerodynamics (Chen *et al.* 2014, Kwok *et al.* 2012, Larose and Mann 1998, Yang *et al.* 2017,

Ma *et al.* 2019 and others). The mean and fluctuating pressures are defined as the mean pressure coefficient C_p and the fluctuating pressure coefficient $C_{p'}$, as shown in Eqs. (13) - (14), respectively.

$$C_p = \frac{P - P_\infty}{0.5\rho U_\infty^2} \quad (13)$$

$$C_{p'} = \frac{P' - P_\infty}{0.5\rho U_\infty^2} \quad (14)$$

where P and P' are the local mean and fluctuating pressure on the girder surface, respectively, and P_∞ is the pressure upstream of the deck.

As shown in Fig. 12, the present mean pressures distribution has a good agreement with the experimental results of Kwok *et al.* (2012). As for the cases of different gap ratios, the mean pressures along the upper surface of upstream girder with all studied gap ratios have similar distribution. It means that the L/C has little influence on the mean pressure distribution on the upper surface of upstream girder as result of the similar flow structure in this region as shown in Fig. 10. The flat pressure distribution appears in rear part of Side B-C, which illustrates that the flow reattachment occurs in those regions with the reattachment length of approximately $1D$. Kwok *et al.* (2012) obtained a similar result in their experimental study. From Fig. 12(b), the magnitude of mean pressures distributions on upper

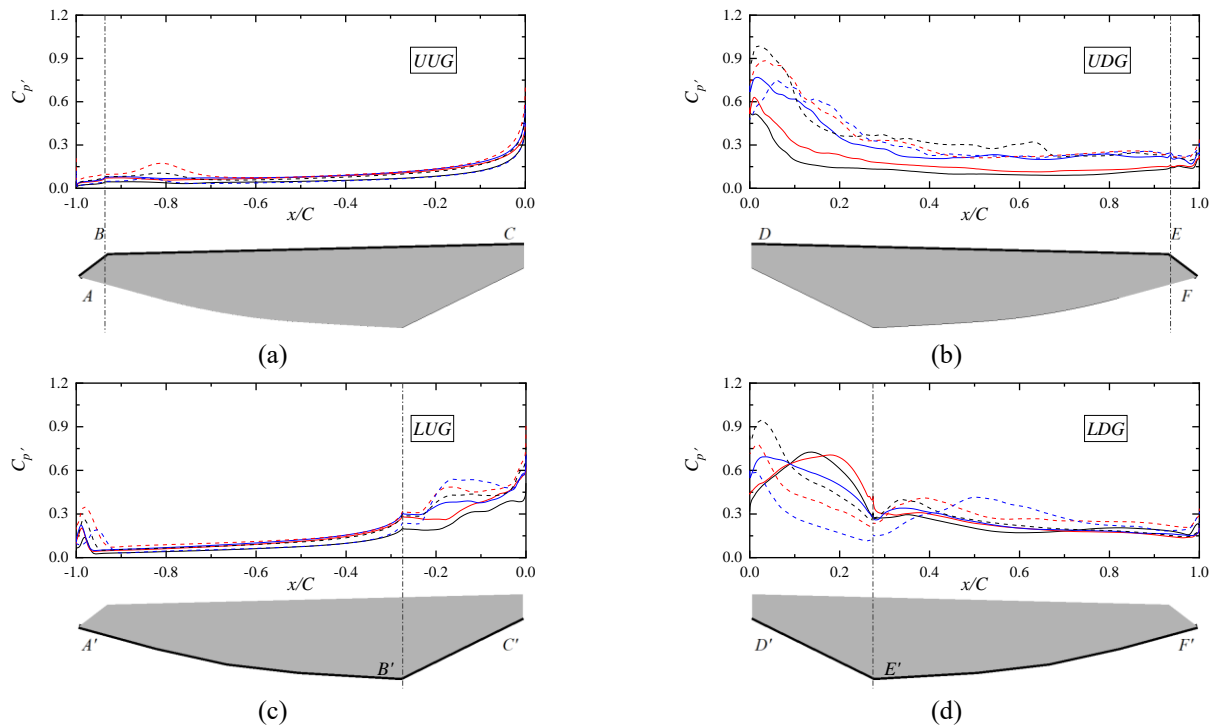


Fig.13 Fluctuating pressure distributions along: (a) UUG, (b) UDG, (c) LUG and (d) LDG

*——: $L/C = 5.1\%$; ———: $L/C = 12.8\%$; ———: $L/C = 25.6\%$; ----: $L/C = 38.5\%$; ----: $L/C = 73.3\%$; ----: $L/C = 108.2\%$.
 surface of downstream girder (Side D-E) increases with distribution on the upper surface of upstream girder with

L/C , and the negative mean pressure occurs on the windward part of Side D-E, which illustrates that the suction force occurs due to a separation bubble as shown in Fig. 10. Due to the change of flow pattern, the mean reattachment lengths on the upper surface of downstream girder in the single-side shedding regime ($L/C=5.1\% \sim 25.6\%$) and co-shedding regime ($L/C=38.5\% \sim 108.2\%$) are $0.75D$ and $2.78D$, respectively. All these variations of mean pressure distribution would have direct effect on the aerodynamic forces.

As shown in Figs 12(c) and 12(d), the mean pressures on the lower surface of upstream girder have a similar tendency with all cases in Side A'-B', as well in Side D'-E', though their values have some differences, which may be caused by the increasing velocity with the L/C . However, there are significant differences for the mean pressure in Sides B'-C' and D'-E', where the distributions can be divided into two patterns. In Sides B'-C', the mean pressure distribution has no peak value for the gap ratios less than 38.5%. However, the peak values can be found in the pressure distributions for the gap ratios of 38.5% to 108.2%, due to the main vortex moving upward to the upstream girder and changing to body-fitted shape. As shown in Fig. 10, if the L/C less than 38.5%, the main vortex with horizontal shape causes a suction which produces negative pressure distributions in Side D'-E'. As the L/C increases to 38.5%, the main vortex vanishes from the windward part of lower surface of downstream girder and the air flows over the Side D'-E', which cause the mean pressure coefficients to change from negative to positive on this surface.

Similarly to the variation of the mean pressure

L/C , the fluctuating pressure distributions presented in Figs. 13(a) and (b) for all studied gap ratios have similar shapes. The fluctuating pressure distribution on the upper surface of downstream girder is sensitive to L/C , where the fluctuating pressure distributions on Side D-E have two shapes, which correspond to the two flow regimes observed. The value of fluctuating pressure in the center vortex regime ($L/C=5.1\% \sim 25.6\%$) increases suddenly to that in the co-shedding regime ($L/C \geq 25.6\%$) because of the impingement of vortices shed from the upstream girder onto the side D-E. In addition, it can be found that the peak value appears at the L/C of 38.5% as in the co-shedding regime. It means that the strength of vortices impinging onto the side D-E increases and decreases within the L/C range of 25.6% ~ 38.5% and 38.5% ~ 108.2%, respectively.

As shown in Figs. 13(c) and 13(d), on the lower surface of upstream girder, the gap has little effect on the fluctuating pressure distributions on Side A'-B' but does greatly affect on Side B'-C'. In Side B'-C', for large gap ratio ($L/C \geq 73.3\%$), the value of fluctuating pressure suddenly peaks, due to the increasing gap would make the vortex closer to Side B'-C' as shown in Fig. 6. In Side D'-E', the position of peak value of fluctuating pressures changes, which is due to the movement of vortices impingement for all studied gap ratios. In Side E'-F', various vortices exist all times, which is the reason of the similarity in the fluctuating pressure distributions.

3.2.2 Mean and fluctuating aerodynamic forces

Fig. 14 presents the variation of mean drag and lift force coefficients with different gap ratios. As mentioned above,

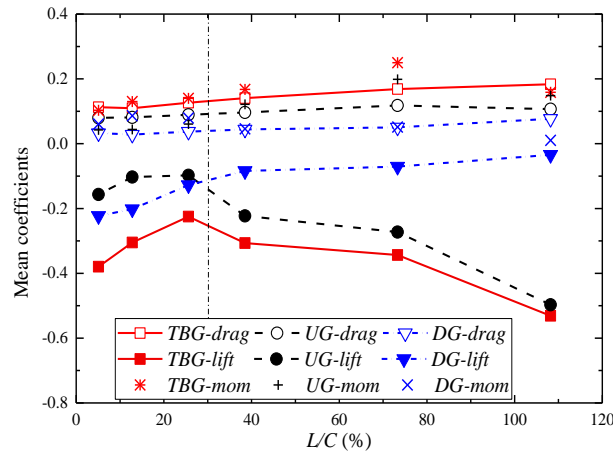


Fig.14 Variation of mean aerodynamic force coefficients with different gap ratios

Note: TBG means the twin box girder; UG means the upstream girder and DG means the downstream girder the L/C has a significant effect on the mean pressure slowly with L/C . In addition, the drag on the downstream

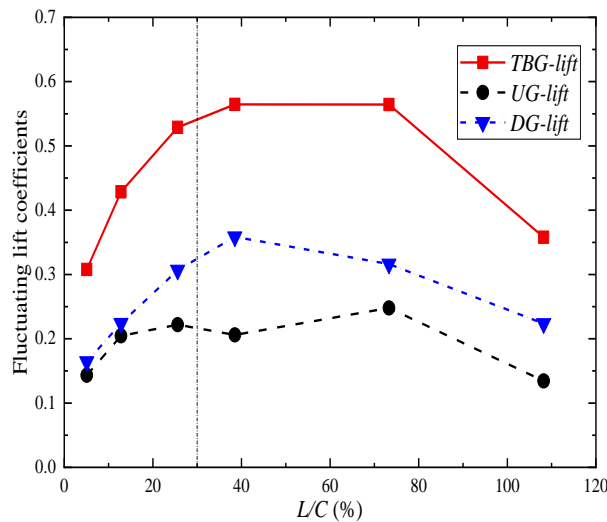


Fig.15 Variation of fluctuating aerodynamic force coefficients with different gap ratios

distributions, especially on those on the lower surface of upstream girder, as well as overall downstream girder. Hence, it is evident that the lift forces on both upstream and downstream girders are quite sensitive to the L/C . In the co-shedding regime ($L/C \geq 38.5\%$), the magnitude of lift on the upstream girder increase with L/C , which attributes to the increase in the negative pressure on the lower surface of upstream girder with the L/C . The increase of L/C is likely to decrease the magnitude of lift on the downstream girder, due to the combination effect of pressure variations on both upper and lower surfaces of downstream girder with L/C as shown in Fig. 12. This effect is also mentioned by Kwok *et al.* (2012). In addition, the total mean lift force of the twin box girder is mainly dominated by the upstream girder. It can be also found that the total moment coefficient in the regime II becomes obvious larger than that in Regime I. From Fig. 14, it can be found that the mean total drag coefficients of all the studied cases are generally quite small as result of the streamlined aerodynamic geometry of the bridge deck, although the mean drags, as well as the mean drags on the upstream and downstream girders increases

girder has been approximately doubled when the L/C increases from 25.6% to 38.5%, although the magnitude remains relatively small, which is also reported in the experimental study of Kwok *et al.* (2012). This is because the increase in the positive pressures on the leading surface of downstream girder with the L/C .

The variation of fluctuating lift coefficients with different gap ratios are presented in Fig. 15. As mentioned above, the effects of L/C are more noticeable on the fluctuating pressure distributions over the downstream girder. The increasing gap ratios are gradually being met by the separation of the shear layers from the upstream girder, thus the alternate vortex shedding occurs in the gap as well as in the wake of the downstream girder, illustrating that the increasing fluctuating lifts.

With the L/C increasing to 38.5%, the interaction between two decks becomes weaker and the vortices strength decreases. Hence the magnitudes of lift on both girders decrease with decreasing L/C , attributing to the evident decrease in the fluctuating pressure distributions on the leading end of Side $D-E$ and Side $D'-E'$ of downstream

girder as the L/C increases, as shown in Fig. 13. In contrast to the mean lift force, the total fluctuating lift force of the twin box girder is mainly dominated by the downstream girder.

4. Conclusions

In present study, 2D DDES simulation is carried out to investigate the uniform flow over a twin-box bridge deck with different gap ratios of $L/C=5.1\%$, 12.8% , 25.6% , 38.5% , 73.3% and 108.2% at Reynolds number, $Re=4\times 10^4$. The numerical method and numerical details applied in this study are validated by comparing the present results to the aerodynamics obtained from wind tunnel test and a previous numerical study at the same Reynolds number. Variations of Strouhal number, unsteady flow structures, pressure distributions and aerodynamic forces with L/C are studied, as well as the interaction and underlying mechanism of the flow around twin-box bridge deck.

Two types of flow patterns with respect to twin-box bridge deck of L/C ranging from 5.1% to 108.2% are observed in the present numerical investigation, i.e. the single-side shedding regime at $L/C\leq 25.6\%$, and co-shedding regime at $L/C\geq 38.5\%$. In the single-side shedding regime, the shear layers separated from upper side of upstream girder reattach onto the upper surface of the downstream girder, and the shear layers separated from lower side of upstream girder form vortices in the gap, which impinge onto the windward and lower sides of downstream girder. In the co-shedding regime, the alternate vortex shedding and the binary vortex street appear in the wakes of upstream and downstream girders, which causes more complex flow interaction between the two girders. Due to the change of flow patterns, the mean reattachment lengths on the upper surface of downstream girder in the single-side shedding and co-shedding regimes are $0.75D$ and $2.78D$, respectively.

The gap-ratio-dependent Strouhal number gradually increases from 0.12 to 0.27 with the L/C , which shows a good general consistency with the experimental results reported in the literature. The dominating frequencies of vortices shedding in the wakes of upstream and downstream girders are almost the same but the main vortex shedding of the twin girders are independent.

The L/C has a significant effect on the mean and fluctuating pressure distributions, especially on those on the lower surface of upstream girder and the whole downstream girder. It is evident that the lift forces on both upstream and downstream girders are quite sensitive to the L/C . As in the co-shedding regime ($L/C\geq 38.5\%$), the magnitude of mean lift on the upstream girder increases with L/C , while an increase of the L/C is likely to decrease the magnitude of mean lift on the downstream girder. The total mean lift force of the twin box girder is mainly dominated by the upstream girder. Things are the opposite for the total fluctuating lift force. The mean total drags of all the studied cases are generally quite small as a result of the streamlined aerodynamic geometry of the bridge deck. The fluctuating lift on the downstream girder increases and decreases with

L/C in the single-side shedding and co-shedding regimes, respectively.

Acknowledgments

This research was funded in part by the Natural Science Foundation of China (NSFC, No. 51708462, 51508333) and the Fundamental Research Funds for the Central Universities (NO.2682016CX006).

References

- Armfield, S. and Street, R. (1999), "The fractional-step method for the navier-stokes equations on staggered grids: the accuracy of three variations", *J. Comput. Phys.*, **153**(2), 660-665. <https://doi.org/10.1006/jcph.1999.6275>.
- Chen, W., Lima, S., Li, H. and Hu, H. (2013). "An experimental study of the unsteady vortex and flow structures around twin-box-girder bridge deck models", *Proceedings of the 31st AIAA Applied Aerodynamics Conference*. <https://doi.org/10.2514/6.2013-2811>.
- Chen, W.L., Li, H. and Hu, H. (2014), "An experimental study on the unsteady vortices and turbulent flow structures around twin-box-girder bridge deck models with different gap ratios", *J. Wind Eng. Ind. Aerod.*, **132**, 27-36. <https://doi.org/10.1016/j.jweia.2014.06.015>.
- Diana, G., Resta, F., Zasso, A., Belloli, M. and Rocchi, D. (2004), "Forced motion and free motion aeroelastic tests on a new concept dynamometric section model of the Messina suspension bridge", *J. Wind Eng. Ind. Aerod.*, **92**(6), 441-462. <https://doi.org/10.1016/j.jweia.2004.01.005>.
- Fumoto, K. and Watanabe, S. (2015), "An estimation of aerodynamics of slotted one-box girder section using computational fluid dynamics", *In Proceedings of the Fourth International Symposium on Computational Wind Engineering*, Yokohama, Japan.
- Ge, Y. and Xiang, H. (2008), "Bluff body aerodynamics application in challenging bridge span length", *In Proceedings of 6th International Colloquium on Bluff Bodies Aerodynamics and Applications*.
- Kim, S. and Makarov, B. (2005), "An implicit fractional-step method for efficient transient simulation of incompressible flows", *Proceedings of the 17th AIAA Computational Fluid Dynamics Conference*.
- Kwok, K.C., Qin, X.R., Fok, C.H. and Hitchcock, P.A. (2012), "Wind-induced pressures around a sectional twin-deck bridge model: Effects of gap-width on the aerodynamic forces and vortex shedding mechanisms", *J. Wind Eng. Ind. Aerod.*, **110**, 50-61. <https://doi.org/10.1016/j.jweia.2012.07.010>.
- Laima, S. and Li, H. (2015), "Effects of gap width on flow motions around twin-box girders and vortex-induced vibrations", *J. Wind Eng. Ind. Aerod.*, **139**, 37-49. <https://doi.org/10.1016/j.jweia.2015.01.009>.
- Larose, G.L. and Mann, J. (1998), "Gust loading on streamlined bridge decks", *J. Fluids Struct.*, **12**(5), 511-536. <https://doi.org/10.1006/jfls.1998.0161>.
- Larsen, A. (1993), "Aerodynamics aspects of the final design of the 1624m suspension bridge across the great belt", *J. Wind Eng. Ind. Aerod.*, **48**(2-3), 261-285. [https://doi.org/10.1016/0167-6105\(93\)90141-A](https://doi.org/10.1016/0167-6105(93)90141-A).
- Larsen, A., Savage, M., Lafrenière, A., Hui, M.C. and Larsen, S.V. (2008), "Investigation of vortex response of a twin box bridge section at high and low Reynolds numbers", *J. Wind Eng. Ind. Aerod.*, **96**(6-7), 934-944.

- <https://doi.org/10.1016/j.jweia.2007.06.020>.
- Leonard, B.P. (1991), "The ULTIMATE conservative difference scheme applied to unsteady one-dimensional advection", *Comput. Methods Appl. Mech. Eng.*, **88**(1), 17-74.
- Li, H., Laima, S., Ou, J., Zhao, X., Zhou, W., Yu, Y. and Liu, Z. (2011), "Investigation of vortex-induced vibration of a suspension bridge with two separated steel box girders based on field measurements", *Eng. Struct.*, **33**(6), 1894-1907. <https://doi.org/10.1016/j.engstruct.2011.02.017>.
- Li, Z., Zhou, Q., Liao, H. and Ma, C. (2018), "Numerical studies of the suppression of vortex-induced vibrations of twin box girders by central grids", *Wind Struct.*, **26**(5), 305-315. <https://doi.org/10.12989/was.2018.26.5.305>.
- Ma, C., Wang, J., Li, Q.S. and Liao, H. (2019), "3D aerodynamic admittances of streamlined box bridge decks", *Eng. Struct.*, **179**(51778545), 321-331. <https://doi.org/10.1016/j.engstruct.2018.11.007>.
- Menter, F.R. (1994), "Two-equation eddy-viscosity turbulence models for engineering applications", *AIAA J.*, **32**(8), 1598-1605.
- Menter, F.R., Kuntz, M. and Langtry, R. (2003), "Ten years of industrial experience with the SST turbulence model", *Turbul. Heat Mass Transf.*, **4**(1), 625-632.
- Nieto, F., Kusano, I., Hernández, S. and Jurado, J.Á. (2010), "CFD analysis of the vortex-shedding response of a twin-box deck cable-stayed bridge", *Proceedings of the Fifth International Symposium on Computational Wind Engineering*.
- Ogawa, K., Shimodoi, H. and Oryu, T. (2002), "Aerodynamic characteristics of a 2-box girder section adaptable for a super-long span suspension bridge", *J. Wind Eng. Ind. Aerod.*, **90**(12-15), 2033-2043. [https://doi.org/10.1016/S0167-6105\(02\)00319-7](https://doi.org/10.1016/S0167-6105(02)00319-7).
- Qin, X.R., Kwok, K.C., Fok, C.H., Hitchcock, P.A. and Xu, Y.L. (2007), "Wind-induced self-excited vibrations of a twin-deck bridge and the effects of gap-width", *Wind Struct.*, **10**(5), 463-479. <https://doi.org/10.12989/was.2007.10.5.463>.
- Sato, H., Kusuhashi, S., Ogi, K.I. and Matsufuji, H. (2000), "Aerodynamic characteristics of super long-span bridges with slotted box girder", *J. Wind Eng. Ind. Aerod.*, **88**(2-3), 297-306. [https://doi.org/10.1016/S0167-6105\(00\)00055-6](https://doi.org/10.1016/S0167-6105(00)00055-6).
- Shur, M.L., Spalart, P.R., Strelets, M.K. and Travin, A.K. (2008), "A hybrid RANS-LES approach with delayed-DES and wall-modelled LES capabilities", *Int. J. Heat Fluid Flow* **29**(6), 1638-1649. <https://doi.org/10.1016/j.ijheatfluidflow.2008.07.001>.
- Sohankar, A. (2008), "Large eddy simulation of flow past rectangular-section cylinders: Side ratio effects", *J. Wind Eng. Ind. Aerod.*, **96**(5), 640-655. <https://doi.org/10.1016/j.jweia.2008.02.009>.
- Sohankar, A. (2012), "A numerical investigation of the flow over a pair of identical square cylinders in a tandem arrangement", *Int. J. Numer. Methods Fluids* **70**(10), 1244-1257. <https://doi.org/10.1016/j.jweia.2008.02.009>.
- Spalart, P.R. (1997), "Comments on the feasibility of LES for wings and on a hybrid RANS/LES approach", *Proceedings of the first AFOSR international conference on DNS/LES*. Greyden Press.
- Spalart, P.R. and Allmaras, S.R. (1992), "A one-equation turbulence model for aerodynamic flows", *In 30th Aerospace Sciences Meeting and Exhibit*.
- Sumner, D. (2010), "Two circular cylinders in cross-flow: A review", *J. Fluids Struct.* **26**(6), 849-899. <https://doi.org/10.1016/j.jfluidstructs.2010.07.001>.
- Yang, Y. and Ge, Y. (2009), "Aerodynamic flutter control for typical girder sections of long-span cable-supported bridges", *Wind Struct.*, **12**(3), 205-217. <https://doi.org/10.12989/was.2009.12.3.205>.
- Yang, Y., Li, M., Ma, C. and Li, S. (2017), "Experimental investigation on the unsteady lift of an airfoil in a sinusoidal streamwise gust", *Phys. Fluids* **29**(5). <https://doi.org/10.1063/1.4984243>.
- Yang, Y., Zhou, R., Ge, Y. and Zhang, L. (2016), "Experimental studies on VIV performance and countermeasures for twin-box girder bridges with various slot width ratios", *J. Fluids Struct.*, **66**, 476-489. <https://doi.org/10.1016/j.jfluidstructs.2016.08.010>.
- Zdravkovich, M.M. (1986), "Discussion: Effect of vibrating upstream cylinder of two circular cylinders in tandem arrangement", *J. Fluids Eng.*, **108**(1972), 383-385. <https://doi.org/10.1115/1.3242592>.
- Zhang, Z., Zhang, X., Yang, Y. and Ge, Y. (2017), "Nonlinear aerodynamic and energy input properties of a twin-box girder bridge deck section", *J. Fluids Struct.*, **74**, 413-426. <https://doi.org/10.1016/j.jfluidstructs.2017.06.016>.
- Zhiwen, L.I.U., Zhengqing, C.H.E.N., Gao, L.I.U. and Xinpeng, S. H.A.O. (2009), "Experimental study of aerodynamic interference effects on aerostatic coefficients of twin deck bridges", *Front. Archit. Civil Eng. China.*, **3**(3), 292-298. <https://doi.org/10.1007/s11709-009-0048-8>.
- Zhou, Y. and Mahbub Alam, M. (2016), "Wake of two interacting circular cylinders: a review", *Int. J. Heat Fluid Flow*, **62**(Part B), 510-537. <https://doi.org/10.1016/j.ijheatfluidflow.2016.08.008>.
- Zhou, Y. and Yiu, M.W. (2006), "Flow structure, momentum and heat transport in a two-tandem-cylinder wake", *J. Fluid Mech.* **548**, 17-48. <https://doi.org/10.1017/S002211200500738X>.
- Zhu, Q. and Xu, Y.L. (2014), "Characteristics of distributed aerodynamic forces on a twin-box bridge deck", *J. Wind Eng. Ind. Aerod.*, **131**, 31-45. <https://doi.org/10.1016/j.jweia.2014.05.003>.

FR